

# Preparation and properties of an $\text{Mn}^{\text{IV}}$ –hydroxide complex: proton and electron transfer at a mononuclear manganese site and its relationship to the oxygen evolving complex within photosystem II†

Cite this: *Chem. Sci.*, 2014, 5, 3064Taketo Taguchi,<sup>a</sup> Kari L. Stone,<sup>b</sup> Rupal Gupta,<sup>c</sup> Benedikt Kaiser-Lassalle,<sup>d</sup> Junko Yano,<sup>\*d</sup> Michael P. Hendrich<sup>\*c</sup> and A. S. Borovik<sup>\*a</sup>

Photosynthetic water oxidation is catalyzed by a  $\text{Mn}_4\text{O}_5\text{Ca}$  cluster with an unprecedented arrangement of metal ions in which a single manganese center is bonded to a distorted  $\text{Mn}_3\text{O}_4\text{Ca}$  cubane-like structure. Several mechanistic proposals describe the unique manganese center as a site for water binding and subsequent formation of a high valent Mn–oxo center that reacts with a M–OH unit ( $\text{M} = \text{Mn}$  or  $\text{Ca}^{\text{II}}$ ) to form the O–O bond. The conversion of low valent Mn–OH<sub>*n*</sub> ( $n = 1, 2$ ) to a Mn–oxo species requires that a single manganese site be able to accommodate several oxidation states as the water ligand is deprotonated. To study these processes, the preparation and characterization of a new monomeric  $\text{Mn}^{\text{IV}}$ –OH complex is described. The  $\text{Mn}^{\text{IV}}$ –OH complex completes a series of well characterized Mn–OH and Mn–oxo complexes containing the same primary and secondary coordination spheres; this work thus demonstrates that a single ligand can support mononuclear Mn complexes spanning four different oxidation states (II through V) with oxo and hydroxo ligands that are derived from water. Moreover, we have completed a thermodynamic analysis based on this series of manganese complexes to predict the formation of high valent Mn–oxo species; we demonstrated that the conversion of a  $\text{Mn}^{\text{IV}}$ –OH species to a  $\text{Mn}^{\text{V}}$ –oxo complex would likely occur *via* a stepwise proton transfer–electron transfer mechanism. The large dissociation energy for the  $\text{Mn}^{\text{IV}}$ O–H bond ( $\sim 95 \text{ kcal mol}^{-1}$ ) diminished the likelihood that other pathways are operative within a biological context. Furthermore, these studies showed that reactions between Mn–OH and Mn–oxo complexes lead to non-productive, one-electron processes suggesting that initial O–O bond formation with the OEC does not involve an Mn–OH unit.

Received 10th February 2014  
Accepted 6th May 2014

DOI: 10.1039/c4sc00453a

www.rsc.org/chemicalscience

<sup>a</sup>Department of Chemistry, University of California-Irvine, 1102 Natural Sciences II, Irvine, CA 92697-2025, USA. E-mail: aborovik@uci.edu; Fax: +1-949-824-8571; Tel: +1-949-824-1510

<sup>b</sup>Department of Chemistry, Benedictine University, Lisle, IL 60532, USA. E-mail: kstone@ben.edu

<sup>c</sup>Department of Chemistry, Carnegie Mellon University, Pittsburgh, PA 15213, USA. E-mail: hendrich@andrew.cmu.edu

<sup>d</sup>Physical Biosciences Division, Lawrence Berkeley National Laboratory, Berkeley, CA 94720, USA. E-mail: jyano@lbl.gov

† Electronic supplementary information (ESI) available: Complete synthetic and preparative methods; EPR spectra of  $[\text{Mn}^{\text{II}}\text{H}_3\text{buea}(\text{OH})]^{2-}$ ,  $[\text{Mn}^{\text{III}}\text{H}_3\text{buea}(\text{OH})]^-$ , and  $[\text{Mn}^{\text{IV}}\text{H}_3\text{buea}(\text{OH})]$  (Fig. S1); EXAFS data (Fig. S2 and S3); electronic absorbance spectra for the comproportionation reaction between  $[\text{Mn}^{\text{II}}\text{H}_3\text{buea}(\text{OH})]^{2-}$  and  $[\text{Mn}^{\text{IV}}\text{H}_3\text{buea}(\text{OH})]$  (Fig. S4); spectral data for the reaction between  $[\text{Mn}^{\text{III}}\text{H}_3\text{buea}(\text{OH})]$  and  $\text{KO}^t\text{Bu}$  (Fig. S5); spectral data for the reaction between  $[\text{Mn}^{\text{V}}\text{H}_3\text{buea}(\text{O})]$  and 2,4,6-tri-*tert*-butylphenol (Fig. S6); and electronic absorbance spectra for the reaction between  $[\text{Mn}^{\text{II}}\text{H}_3\text{buea}(\text{OH})]^{2-}$  and  $[\text{Mn}^{\text{IV}}\text{H}_3\text{buea}(\text{O})]^-$  (Fig. S7). See DOI: 10.1039/c4sc00453a

## Introduction

Photosynthetic oxidation of water to dioxygen is an essential reaction that requires the precise transfer of four protons and four electrons during turnover. The enzyme photosystem II that catalyzes this reaction uses a metallocluster composed of one calcium and four manganese ions (referred to as the oxygen evolving complex, OEC), in which all of the metal centers contained within the cluster are essential for function.<sup>1</sup> The arrangement of metal ions within the OEC is approximated by a model having one of the manganese centers bonded to a  $\text{Mn}_3\text{O}_4\text{Ca}$  cubane-like structure.<sup>2</sup> This lone, “dangling” manganese ion (denoted  $\text{Mn}_{\text{A4}}$ ) has a highly anionic primary coordination sphere and appears to be capable of binding water molecules. Structural studies have shown that  $\text{Mn}_{\text{A4}}$  is located close to the calcium ion and that their primary coordination spheres are connected through bridging hydroxo or oxo ligands. The secondary coordination spheres surrounding the Mn–( $\mu\text{-O}(\text{H})$ )–Ca unit are also linked *via* a network of intramolecular

hydrogen bonds.<sup>2</sup> To facilitate the conversion of two water molecules to dioxygen, the OEC assembles oxidizing equivalents through 5 different redox states (denoted S-states within the so-called Kok cycle) with the most oxidizing being the transient S<sub>4</sub> state, which oxidizes water molecules and converts back to the most reduced S<sub>0</sub> state. The structure of the S<sub>4</sub> state is still not known, which has complicated delineation of the mechanism for water oxidation. Nevertheless, several proposals involve a high valent Mn-oxo center (formally a Mn<sup>V</sup>-oxo site) within the S<sub>4</sub> state and this species has a direct role in the water oxidation process (Fig. 1).<sup>1f,3</sup> The conversion to a high-valent Mn-oxo center probably precedes through controlled oxidation/proton-loss processes from Mn-OH<sub>2</sub>/Mn-OH species that are present in the reduced S states. For instance, the S<sub>3</sub> → S<sub>4</sub> step could reasonably involve the transformation of a Mn<sup>IV</sup>-OH species to a Mn<sup>V</sup>-oxo unit (Fig. 1).<sup>1f,4</sup>

The applicability of the pathway depicted in Fig. 1 necessitates that a single manganese-aquo center can traverse at least two oxidation states to form a Mn<sup>V</sup>-oxo species within the OEC; this species must then be able to facilitate a two-electron event involving the coupling of oxo and hydroxo ligands during initial O-O bond formation. To investigate these issues, we have examined the chemistry within a series of synthetic Mn-O(H) complexes.<sup>5</sup> An advantage of this approach is that it allows us to probe the intrinsic properties associated with monomeric Mn-O(H) complexes, including an analysis that describes the thermodynamic relationships between the Mn-oxo and Mn-hydroxo complexes. Our previous work has described the formation of monomeric, high-spin Mn-oxo complexes that span three oxidation states (Chart 1).<sup>5</sup> The complexes are prepared from water and use the ligand tris[(*N'*-*tert*-butylureaylato)-*N*-ethylene]aminato ([H<sub>3</sub>buea]<sup>3-</sup>) that provides an intramolecular hydrogen bonding network around the metal center; these complexes thus serve as an approximate single-site representation for the lone high-valent Mn-oxo center in the OEC.<sup>1,2,6</sup> We have also prepared two related monomeric Mn<sup>III</sup>-OH and Mn<sup>II</sup>-OH complexes, and in this report we describe a new Mn<sup>IV</sup>-OH complex, [Mn<sup>IV</sup>H<sub>3</sub>buea(OH)]. Monomeric Mn<sup>IV</sup> complexes with a terminal hydroxo ligand are rare, and the few that have been characterized are limited to the Mn<sup>IV</sup>-(OH)<sub>2</sub> complexes of Busch and Costas, and the Mn<sup>IV</sup>-OH species of Goldberg, Fujii, and Anxolabéhère-Mallart.<sup>7-9</sup> Our studies demonstrate that conversion of Mn<sup>IV</sup>-OH to a Mn<sup>V</sup>-oxo center can readily occur *via* a mechanism involving discrete proton transfer-electron transfer (PT-ET) steps. Furthermore, we obtained experimental evidence for the reactivity between Mn-

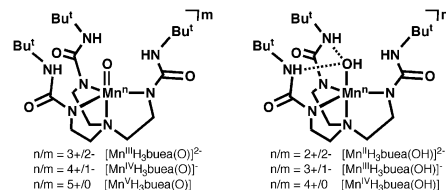


Chart 1

oxo and Mn-OH complexes that argue against the involvement of a Mn-OH species in O-O bond formation during photosynthetic water oxidation.

## Results

See ESI for full experimental details.†

### Conversion of Mn<sup>III</sup>-OH to Mn<sup>IV</sup>-OH: oxidation route

We have reported the isolation and characterization of [Mn<sup>II</sup>H<sub>3</sub>buea(OH)]<sup>2-</sup> and [Mn<sup>III</sup>H<sub>3</sub>buea(OH)]<sup>-</sup> and have used these complexes to investigate the preparation of a Mn<sup>IV</sup>-OH complex (Chart 1).<sup>5a,b</sup> The synthetic accessibility of [Mn<sup>IV</sup>H<sub>3</sub>buea(OH)] was explored using cyclic voltammetry; previous measurements on [Mn<sup>III</sup>H<sub>3</sub>buea(OH)]<sup>-</sup> at room temperature in DMSO produced a quasi-reversible reductive process at -1.5 V and an irreversible oxidative process at -0.18 V.<sup>10</sup> However, when the data were collected at -60 °C in DMF, the oxidative process became quasi-reversible at an *E*<sub>1/2</sub> = -0.15 V (Fig. 2A). We assigned this feature to the Mn<sup>IV</sup>/Mn<sup>III</sup>-OH couple and anticipated that the corresponding Mn<sup>IV</sup>-OH species could be stabilized at lower temperatures. To further probe this redox process, we spectrophotometrically monitored the stepwise oxidation of [Mn<sup>II</sup>H<sub>3</sub>buea(OH)]<sup>2-</sup> (Scheme 1) at -80 °C in 1 : 1 THF : DMF (Fig. 2B). The addition of one equivalent of [FeCp<sub>2</sub>]<sup>+</sup> to the colorless [Mn<sup>II</sup>H<sub>3</sub>buea(OH)]<sup>2-</sup> solution produced the absorbance spectrum of [Mn<sup>III</sup>H<sub>3</sub>buea(OH)]<sup>-</sup> with bands at λ<sub>max</sub> = 431 and 716 nm that are nearly identical to those found for the complex at room temperature. Treatment of this [Mn<sup>III</sup>H<sub>3</sub>buea(OH)]<sup>-</sup> solution with another equivalent of [FeCp<sub>2</sub>]<sup>+</sup> caused the disappearance of these features and the appearance of a new peak at λ<sub>max</sub>/nm (ε<sub>M</sub>/M<sup>-1</sup> cm<sup>-1</sup>) = 466 (5700) that is stable for hours at -80 °C. This new band is

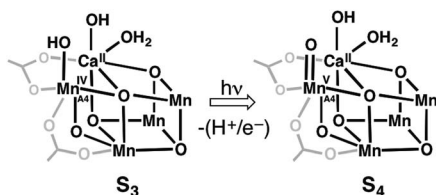


Fig. 1 A hypothetical depiction of the S<sub>3</sub> state converting to the S<sub>4</sub> state in the OEC that involves a high valent Mn site.

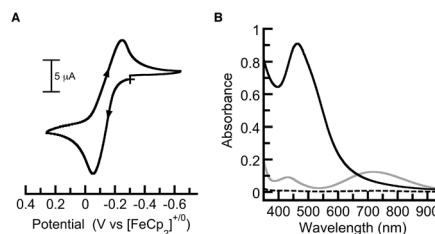


Fig. 2 (A) Cyclic voltammogram of [Mn<sup>III</sup>H<sub>3</sub>buea(OH)]<sup>-</sup> recorded at -60 °C in DMF at a scan rate of 0.01 V s<sup>-1</sup>. (B) Electronic absorbance spectra of [Mn<sup>II</sup>H<sub>3</sub>buea(OH)]<sup>2-</sup> (black, dashed), [Mn<sup>III</sup>H<sub>3</sub>buea(OH)]<sup>-</sup> (gray), and [Mn<sup>IV</sup>H<sub>3</sub>buea(OH)] (black, solid) collected at -80 °C in 1 : 1 THF : DMF.



Scheme 1 Conditions: (a) 1.0 equiv.  $[\text{FeCp}_2]^+$ , 1 : 1 DMF : THF,  $-80^\circ\text{C}$ .

assigned to the optical feature associated with the  $\text{Mn}^{\text{IV}}\text{-OH}$  complex,  $[\text{Mn}^{\text{IV}}\text{H}_3\text{buea}(\text{OH})]$ .

The oxidation of  $[\text{Mn}^{\text{II}}\text{H}_3\text{buea}(\text{OH})]^{2-}$  was also studied using parallel ( $B_{\parallel}|B$ ) and perpendicular ( $B_{\perp}|B$ ) mode electron paramagnetic resonance (EPR) spectroscopy (Fig. S1†). The  $[\text{Mn}^{\text{II}}\text{H}_3\text{buea}(\text{OH})]^{2-}$  species showed signals at  $g = 5.17$ , 1.80, 1.37 in perpendicular mode and at  $g = 4.60$  in parallel mode (Fig. S1A and D†). The addition of 1 equiv. of  $[\text{FeCp}_2]^+$  resulted in the loss of signals from  $[\text{Mn}^{\text{II}}\text{H}_3\text{buea}(\text{OH})]^{2-}$  and the appearance of a 6-line hyperfine pattern centered at  $g = 8.14$  ( $A = 270$  MHz,  $a = 9.6$  mT) in parallel mode (Fig. S1E†). This pattern originates from an  $S = 2$  spin ground state that is assigned to  $[\text{Mn}^{\text{III}}\text{H}_3\text{buea}(\text{OH})]^-$ .<sup>11</sup> Addition of a second equivalent of  $[\text{FeCp}_2]^+$  resulted in the loss of the 6-line pattern from the  $\text{Mn}^{\text{III}}\text{-OH}$  complex in parallel mode and the appearance of signals in perpendicular mode (Fig. S1C†) at  $g = 5.47$ , 2.95, 1.43.<sup>12</sup> The positions of these resonances are indicative of an  $S = 3/2$  spin-state, which is assigned to the  $[\text{Mn}^{\text{IV}}\text{H}_3\text{buea}(\text{OH})]$  complex.<sup>13</sup> These EPR results show the near quantitative conversion of  $\text{Mn}^{\text{II}}\text{-OH}$  complex to  $\text{Mn}^{\text{III}}\text{-OH}$  complex, which then was oxidized to the  $\text{Mn}^{\text{IV}}\text{-OH}$  complex. We have previously reported the EPR properties of the  $\text{Mn}^{\text{IV}}\text{=O}$  complexes with  $[\text{H}_3\text{buea}]^{3-}$ , which also has an  $S = 3/2$  ground spin state. However, the EPR signal corresponding to  $[\text{Mn}^{\text{IV}}\text{H}_3\text{buea}(\text{O})]$  is distinctly different from that found for the  $[\text{Mn}^{\text{IV}}\text{H}_3\text{buea}(\text{OH})]$  complex.<sup>5c</sup> A detailed analysis of the EPR properties for the three  $\text{Mn-OH}$  complexes has been described in a separate report.<sup>14</sup>

### X-ray absorption spectroscopy

The manganese K-edge X-ray absorption spectra (XAS) of the three  $\text{Mn-OH}$  complexes were measured to evaluate their structural properties. X-ray absorption near-edge absorption spectra (XANES) collected on  $[\text{Mn}^{\text{II}}\text{H}_3\text{buea}(\text{OH})]^{2-}$ ,  $[\text{Mn}^{\text{III}}\text{H}_3\text{buea}(\text{OH})]^-$  and  $[\text{Mn}^{\text{IV}}\text{H}_3\text{buea}(\text{OH})]$  showed edge-energy shifts of  $\sim 2.5$  eV ( $\text{Mn}(\text{II})$  to  $\text{Mn}(\text{III})$ ) and  $\sim 3.3$  eV ( $\text{Mn}(\text{III})$  to  $\text{Mn}(\text{IV})$ ) by the 1st inflection point energy in the spectra, which support the sequential oxidation of the manganese center (Fig. 3). The rising edge-energy taken from the 2<sup>nd</sup> derivative

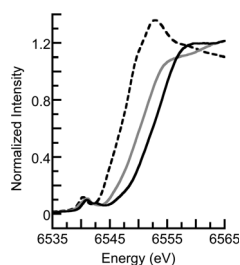


Fig. 3 XANES spectra of  $[\text{Mn}^{\text{II}}\text{H}_3\text{buea}(\text{OH})]^{2-}$  (black, dashed),  $[\text{Mn}^{\text{III}}\text{H}_3\text{buea}(\text{OH})]^-$  (gray), and  $[\text{Mn}^{\text{IV}}\text{H}_3\text{buea}(\text{OH})]$  (black, solid) collected at 10 K in 1 : 1 THF : DMF.

spectrum was 6548.00 eV for  $[\text{Mn}^{\text{II}}\text{H}_3\text{buea}(\text{OH})]^{2-}$ , 6550.55 eV for  $[\text{Mn}^{\text{III}}\text{H}_3\text{buea}(\text{OH})]^-$ , and 6553.84 eV for  $[\text{Mn}^{\text{IV}}\text{H}_3\text{buea}(\text{OH})]$ .

Findings from EXAFS studies (Fig. S2 & S3;† Table 1) also support the step-wise oxidation of  $[\text{Mn}^{\text{II}}\text{H}_3\text{buea}(\text{OH})]^{2-}$  to its analogous  $\text{Mn}^{\text{III}}\text{-OH}$  and  $\text{Mn}^{\text{IV}}\text{-OH}$  complexes. We have previously determined the molecular structures of  $[\text{Mn}^{\text{II}}\text{H}_3\text{buea}(\text{OH})]^{2-}$  and  $[\text{Mn}^{\text{III}}\text{H}_3\text{buea}(\text{OH})]^-$  using single-crystal X-ray diffraction (XRD) methods and have used these results to aid in our analysis of the EXAFS data. From the XRD studies,  $[\text{Mn}^{\text{II}}\text{H}_3\text{buea}(\text{OH})]^{2-}$  has a trigonal bipyramidal structure with three distinct types of Mn-X bonds (Table 1): a Mn-O(H) bond distance at 2.06 Å, three Mn- $\text{N}_{\text{urea}}$  bond distances between 2.13 to 2.18 Å, and a long Mn- $\text{N}_{\text{apical}}$  bond length at 2.32 Å. The EXAFS results for  $[\text{Mn}^{\text{II}}\text{H}_3\text{buea}(\text{OH})]^{2-}$  agree with those obtained from XRD. The best fit of the EXAFS data for a five-coordinate complex gave one Mn-O bond length at 2.02 Å, three Mn-N bond distances at 2.15 Å, and one slightly longer Mn-N bond at a distance of 2.19 Å that we have assigned to the Mn- $\text{N}_{\text{apical}}$  bond. Significant changes in the Mn-X bond distances were found upon oxidation to  $[\text{Mn}^{\text{III}}\text{H}_3\text{buea}(\text{OH})]^-$ , particularly the shortening of the Mn-O(H) bond distance to 1.84 Å. In addition, the EXAFS analysis indicated four Mn-N bond lengths of 2.04 Å, suggesting that the  $\text{Mn}^{\text{III}}\text{-OH}$  complex remained five-coordinate. Note that the bond distances obtained for  $[\text{Mn}^{\text{III}}\text{H}_3\text{buea}(\text{OH})]^-$  from the EXAFS study are similar to those found by XRD methods (Table 1). The EXAFS analysis for  $[\text{Mn}^{\text{IV}}\text{H}_3\text{buea}(\text{OH})]$  revealed that the  $\text{N}_4\text{O}$  primary coordination sphere is retained upon oxidation to the  $\text{Mn}^{\text{IV}}\text{-OH}$  complex. An Mn-O bond distance of 1.83 Å was found for  $[\text{Mn}^{\text{IV}}\text{H}_3\text{buea}(\text{OH})]$ , which is statistically the same as that determined for  $[\text{Mn}^{\text{III}}\text{H}_3\text{buea}(\text{OH})]^-$ . Moreover, the EXAFS data were fit to 4 Mn-N bond distances at 1.97 Å, which represents a contraction of 0.07 Å from those observed in  $[\text{Mn}^{\text{III}}\text{H}_3\text{buea}(\text{OH})]^-$ .

The EXAFS data agree with theoretical predictions for complexes with localized trigonal symmetry that possess two

Table 1 EXAFS fitting parameters obtained for  $[\text{Mn}^{\text{II}}\text{H}_3\text{buea}(\text{OH})]^{2-}$  (1),  $[\text{Mn}^{\text{III}}\text{H}_3\text{buea}(\text{OH})]^-$  (2), and  $[\text{Mn}^{\text{IV}}\text{H}_3\text{buea}(\text{OH})]$  (3)

	Shell	N	$R \text{ \AA}^{-1}$			R/%
			XRD	EXAFS	$\sigma^2/\text{\AA}^2$	
1	Mn-O	1	2.06	2.02	0.003	$1.0E_0$ (eV) = 4.3
	Mn-N	3	2.13–2.18	2.15	0.004	
	Mn-N	1	2.32	2.19	0.002	
	Mn-C	9	3.04–3.20	3.09	0.009	
	Mn-C-N	18	3.32–3.44	3.39	0.013	
2	Mn-N	3	3.31–3.37	3.37	0.021	$4.9E_0$ (eV) = 7.7
	Mn-O	1	1.88	1.84	0.003	
	Mn-N	4	2.01–2.07	2.04	0.005	
	Mn-C	9	2.80–3.14	3.00	0.017	
	Mn-C-N	18	3.15–3.25	3.31	0.008	
3	Mn-N	3	3.28–3.38	3.33	0.004	$0.7E_0$ (eV) = 6.6
	Mn-O	1		1.83	0.003	
	Mn-N	4		1.97	0.005	
	Mn-C	9		2.94	0.015	
	Mn-C-N	18		3.45	0.020	
	Mn-N	3		3.25	0.003	

degenerate sets of d orbitals: the  $d_{xz}$ ,  $d_{yz}$  orbitals with  $\pi^*$  character along the Mn–O bond and the  $d_{xy}$ ,  $d_{x^2-y^2}$  orbitals having  $\sigma^*$  character within the trigonal plane.<sup>15</sup> The  $d_{z^2}$  orbital is at higher energy and has  $\sigma^*$  character along the Mn–O bond. The one-electron oxidation of  $[\text{Mn}^{\text{II}}\text{H}_3\text{buea}(\text{OH})]^{2-}$  ( $S = 5/2$ ) caused a significant contraction of the Mn–O bond in the resulting  $\text{Mn}^{\text{III}}\text{–OH}$  complex because an electron was removed from the  $d_{z^2}$  orbital. Further oxidation to  $[\text{Mn}^{\text{IV}}\text{H}_3\text{buea}(\text{OH})]$  lead to negligible changes in the Mn–O bond length but a measurable shortening of the Mn–N<sub>urea</sub> bonds, which is consistent with the removal of an electron from the degenerate  $d_{xy}$ ,  $d_{x^2-y^2}$  orbitals.<sup>16</sup> These observations are similar to those reported by Smith on a series of Fe–nitrido complexes.<sup>17</sup>

### Thermodynamic cycles for the Mn–OH and Mn–oxo complexes

The preparation of  $[\text{Mn}^{\text{IV}}\text{H}_3\text{buea}(\text{OH})]$  extends our series of monomeric Mn–OH complexes, and together with the related Mn–oxo complexes, allowed us to assess the intrinsic properties of complexes with Mn–O(H) moieties. In particular, studies on these complexes allowed us to construct three related thermodynamic cycles that aided in predicting the reactivity of the Mn–O(H) complexes (Fig. 4).<sup>18</sup> We have previously reported estimates for the O–H bond dissociation energies ( $\text{BDE}_{\text{OH}}$ ) for  $[\text{Mn}^{\text{II}}\text{H}_3\text{buea}(\text{OH})]^{2-}$  and  $[\text{Mn}^{\text{III}}\text{H}_3\text{buea}(\text{OH})]^-$  as 77 and 89 kcal mol<sup>−1</sup>, respectively<sup>19</sup> and now have added the value for  $[\text{Mn}^{\text{IV}}\text{H}_3\text{buea}(\text{OH})]$ , which is 95 kcal mol<sup>−1</sup>. The  $\text{BDE}_{\text{OH}}$  values show the expected increase in  $\text{BDE}_{\text{OH}}$  with increasing oxidation state of the metal center. We are unaware of a similar experimental study to evaluate  $\text{BDE}_{\text{OH}}$  values for metal–hydroxo complexes spanning three oxidation states. Normally, this information is applied toward processes involving organic substrates bearing X–H bonds;<sup>18</sup> however, we have used these thermodynamic relationships to guide reactivity studies between the Mn–OH and Mn–oxo complexes.<sup>20</sup>

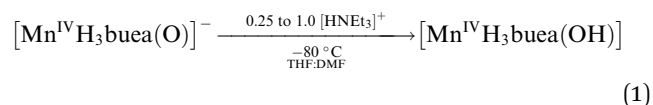
### Comproportionation reaction

If our assignment of the  $[\text{Mn}^{\text{IV}}\text{H}_3\text{buea}(\text{OH})]$  complex is correct, we reasoned that a comproportionation reaction should occur between the  $\text{Mn}^{\text{II}}\text{–OH}$  and  $\text{Mn}^{\text{IV}}\text{–OH}$  complexes to produce  $[\text{Mn}^{\text{III}}\text{H}_3\text{buea}(\text{OH})]^-$ , which has known spectroscopic

properties. We successfully tested this premise by mixing equimolar amounts of  $[\text{Mn}^{\text{II}}\text{H}_3\text{buea}(\text{OH})]^{2-}$  and  $[\text{Mn}^{\text{IV}}\text{H}_3\text{buea}(\text{OH})]$  to produce  $[\text{Mn}^{\text{III}}\text{H}_3\text{buea}(\text{OH})]^-$ , whose concentration was twice that of the starting species. This reaction was verified spectrophotometrically, in which the final product had the exact absorbance spectrum of  $[\text{Mn}^{\text{III}}\text{H}_3\text{buea}(\text{OH})]^-$  (Fig. S4†). Moreover, the reaction was monitored using parallel and perpendicular mode EPR spectroscopy (Fig. 5A & B). We observed the conversion of signals in the perpendicular mode EPR spectra for the  $\text{Mn}^{\text{II}}\text{–OH}$  and  $\text{Mn}^{\text{IV}}\text{–OH}$  complexes to a single, 6-line hyperfine signal at  $g = 8.14$  in parallel mode. The quantitative comproportionation reaction also indicates that the molecular structure is not irreversibly disrupted upon oxidation to  $\text{Mn}^{\text{IV}}\text{–OH}$ .

### Conversion of $\text{Mn}^{\text{IV}}\text{–oxo}$ to $\text{Mn}^{\text{IV}}\text{–OH}$ : protonation route

To further support the identity of  $[\text{Mn}^{\text{IV}}\text{H}_3\text{buea}(\text{OH})]$ , we have employed a protonation approach that utilizes the related  $\text{Mn}^{\text{IV}}\text{–oxo}$  complex (Chart 1). Our thermodynamic evaluation suggested that the oxo ligand should be readily protonated (Fig. 4). Thus, treating  $[\text{Mn}^{\text{IV}}\text{H}_3\text{buea}(\text{O})]^-$  with  $[\text{HNEt}_3]^+$  in 1 : 1 THF : DMF at  $-80^\circ\text{C}$  produced the expected  $[\text{Mn}^{\text{IV}}\text{H}_3\text{buea}(\text{OH})]$  species (eqn (1)). Following this reaction spectrophotometrically showed clean conversion from the  $\text{Mn}^{\text{IV}}\text{–oxo}$  complex to  $[\text{Mn}^{\text{IV}}\text{H}_3\text{buea}(\text{OH})]$  with two isosbestic points at  $\lambda = 437$  and  $583$  nm (Fig. 6A). This result was corroborated using EPR spectroscopy, in which the distinct  $S = 3/2$  spectrum for  $[\text{Mn}^{\text{IV}}\text{H}_3\text{buea}(\text{O})]^-$  is converted to that of  $[\text{Mn}^{\text{IV}}\text{H}_3\text{buea}(\text{OH})]$  upon addition of acid (Fig. 6B).



The deprotonation of  $[\text{Mn}^{\text{IV}}\text{H}_3\text{buea}(\text{OH})]$  was also investigated *via* the reaction of  $[\text{Mn}^{\text{IV}}\text{H}_3\text{buea}(\text{OH})]$  with *tert*-butoxide ion at  $-80^\circ\text{C}$  in 1 : 1 THF : DMF. Both UV-vis and EPR spectroscopies conclusively showed that  $[\text{Mn}^{\text{IV}}\text{H}_3\text{buea}(\text{OH})]$  could

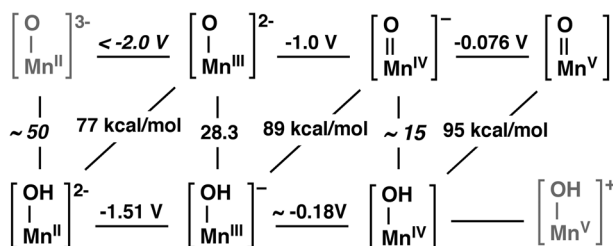


Fig. 4 Thermodynamic cycles developed in DMSO to evaluate the  $\text{BDE}_{\text{OH}}$  with redox potentials referenced to the  $[\text{FeCp}_2]^+ / [\text{FeCp}_2]$  couple. Key: vertical lines,  $\text{pK}_a$  values; horizontal lines, redox potentials; and diagonal lines,  $\text{BDE}_{\text{OH}}$ . Complex in black have been detected and characterized. Values in italics are estimates.

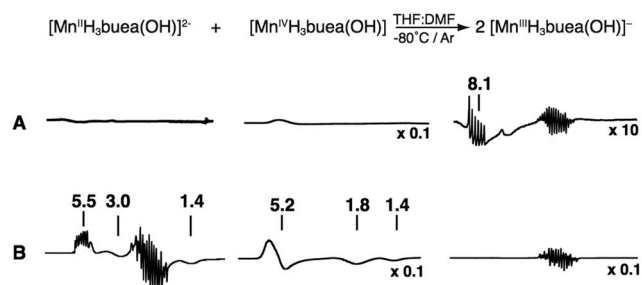


Fig. 5 Comproportionation reaction between 10 mM solutions of  $[\text{Mn}^{\text{II}}\text{H}_3\text{buea}(\text{OH})]^{2-}$  and  $[\text{Mn}^{\text{IV}}\text{H}_3\text{buea}(\text{OH})]$ : EPR spectra (A) with  $\text{B1} \parallel \text{B}$  and (B) with  $\text{B1} \perp \text{B}$ . Experimental conditions: temperature 10 K, power 0.2 mW, frequency 9.6 GHz ( $\text{B1} \perp \text{B}$ ), 9.3 ( $\text{B1} \parallel \text{B}$ ) GHz. The relative scales of the spectra are indicated. The multi-line signals at  $g \sim 2$  are from small impurities that account for less than 2% of the total manganese in the samples.



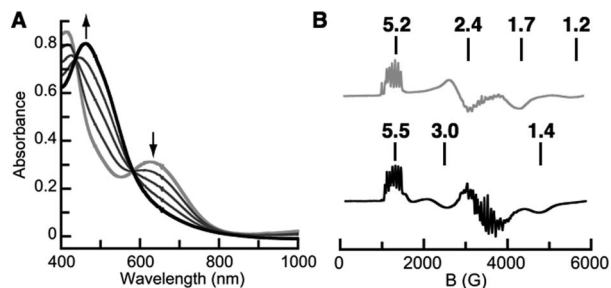
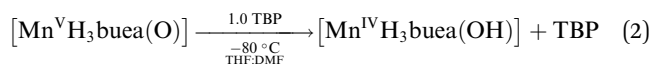


Fig. 6 Experimental data for the reaction shown in eqn (2): (A) electronic absorbance spectra collected at  $-80\text{ }^{\circ}\text{C}$  in 1 : 1 THF : DMF for  $[\text{Mn}^{\text{IV}}\text{H}_3\text{buea}(\text{O})]^-$  (gray) and after the addition of 0.25, 0.5, 0.75, 1.0 (black) equiv. of  $\text{H}^+$  to  $[\text{Mn}^{\text{IV}}\text{H}_3\text{buea}(\text{O})]^-$ . (B) Perpendicular-mode ( $B_1 \perp B$ ) EPR spectra of  $[\text{Mn}^{\text{IV}}\text{H}_3\text{buea}(\text{O})]^-$  (gray) and after the addition of 1.0 equiv. of  $\text{H}^+$  to  $[\text{Mn}^{\text{IV}}\text{H}_3\text{buea}(\text{O})]^-$  to form  $[\text{Mn}^{\text{IV}}\text{H}_3\text{buea}(\text{OH})]$  (black). Experimental conditions for the EPR measurements: 1 : 1 THF : DMF, temperature 77 K, frequency 9.6 GHz.

be converted to  $[\text{Mn}^{\text{IV}}\text{H}_3\text{buea}(\text{O})]^-$  (Fig. S5†). Taken together, these results demonstrate the reversibility of the protonation/deprotonation process, which is additional evidence to suggest that the  $\text{Mn}^{\text{IV}}$ -oxo and  $\text{Mn}^{\text{IV}}$ -OH complexes have similar molecular structures.

#### Conversion of $\text{Mn}^{\text{V}}$ -oxo to $\text{Mn}^{\text{IV}}$ -OH: PCET route

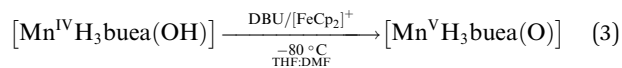
The high-spin  $\text{Mn}^{\text{V}}$ -oxo complex  $[\text{Mn}^{\text{V}}\text{H}_3\text{buea}(\text{O})]$  should serve as a synthon for the formation of the  $\text{Mn}^{\text{IV}}$ -OH complex *via* a proton-coupled electron transfer (PCET) route. The  $\text{BDE}_{\text{OH}} = 95\text{ kcal mol}^{-1}$  estimated for  $[\text{Mn}^{\text{IV}}\text{H}_3\text{buea}(\text{OH})]$  provided a thermodynamic basis for predicting this type of reactivity (Fig. 4). In one study, treating  $[\text{Mn}^{\text{V}}\text{H}_3\text{buea}(\text{O})]$  with 2,4,6-tri-*tert*-butylphenol (TBP,  $\text{BDE}_{\text{OH}} = 80\text{ kcal mol}^{-1}$ )<sup>21</sup> at  $-80\text{ }^{\circ}\text{C}$  cleanly afforded  $[\text{Mn}^{\text{IV}}\text{H}_3\text{buea}(\text{OH})]$  with sharp isosbestic points at  $\lambda = 494$  and  $563\text{ nm}$  (eqn (2), Fig. S6A†). Furthermore, dual-mode EPR spectroscopy showed that the  $S = 1$  signal for  $\text{Mn}^{\text{V}}$ -oxo observed in parallel mode disappeared with concomitant appearance of the  $S = 3/2$  signals for the  $\text{Mn}^{\text{IV}}$ -OH complex when measured in perpendicular mode (Fig. S6B†). An additional EPR feature was observed at  $g = 2$ , which is assigned to the phenoxy radical that was also produced during the reaction.



#### Conversion of $\text{Mn}^{\text{IV}}$ -OH to $\text{Mn}^{\text{V}}$ -oxo: stepwise PT-ET route

We have also studied the reverse reaction involving the conversion of  $[\text{Mn}^{\text{IV}}\text{H}_3\text{buea}(\text{OH})]$  to  $[\text{Mn}^{\text{V}}\text{H}_3\text{buea}(\text{O})]$ . Our thermodynamic estimates suggested that it was unlikely for this conversion to occur *via* homolytic cleavage of the  $\text{MnO-H}$  bond because of its large bond dissociation energy (Fig. 4). We have been unable to determine the redox potential for the one-electron oxidation of  $[\text{Mn}^{\text{IV}}\text{H}_3\text{buea}(\text{OH})]$  but found that  $[\text{FeCp}_2]^+$  at  $-80\text{ }^{\circ}\text{C}$  was unable to perform the oxidation. However, clean formation of  $[\text{Mn}^{\text{V}}\text{H}_3\text{buea}(\text{O})]$  was achieved after this reaction mixture was treated with the base 1,8-diazabicyclo[5.4.0]undec-7-ene (DBU). Isosbestic points at  $\lambda = 490$  and  $570\text{ nm}$  were

observed when this reaction was monitored spectrophotometrically (eqn (3), Fig. 7).



These results are consistent with a step-wise process in which deprotonation of  $[\text{Mn}^{\text{IV}}\text{H}_3\text{buea}(\text{OH})]$  initially occurs to form  $[\text{Mn}^{\text{IV}}\text{H}_3\text{buea}(\text{O})]^-$  that can then be oxidized by  $[\text{FeCp}_2]^+$  to form the desired  $\text{Mn}^{\text{V}}$ -oxo complex. We did not observe intermediates for this process, suggesting that proton transfer was rate limiting.

#### Reactivity between $\text{Mn}$ -oxo and $\text{Mn}$ -OH complexes

We also examined whether two manganese centers could facilitate a two-electron redox event involving the coupling of oxo and hydroxo ligands to form an O-O bond (Fig. 8, path 2). A nucleophilic process has been postulated as one of the many possible routes to the oxidation of water to dioxygen in the OEC<sup>1f,3,22</sup> and  $\text{Mn-OH}$  centers are known to function as nucleophiles in other metalloproteins.<sup>23</sup> However, competitive *one-electron* processes are common for 3d transition metal complexes and could possibly hinder this type of reaction (Fig. 8, path 1).<sup>24</sup> In fact, our thermodynamic analysis indicated that  $\text{Mn}$ -oxo complexes have a strong driving force to undergo one-electron processes that can prevent  $\text{Mn-OH}$  complexes from functioning as a nucleophile in the presence of a high-valent  $\text{Mn}$ -oxo center. We tested the prediction that one-electron processes are likely by investigating the reactivity of our high-valent  $\text{Mn}$ -oxo complexes with the various  $\text{Mn-OH}$  species. For example, an immediate reaction ensued when  $[\text{Mn}^{\text{V}}\text{H}_3\text{buea}(\text{O})]$  was treated with  $[\text{Mn}^{\text{III}}\text{H}_3\text{buea}(\text{OH})]^-$  at  $-80\text{ }^{\circ}\text{C}$ , producing a 45(5) : 55(5) mixture of  $[\text{Mn}^{\text{IV}}\text{H}_3\text{buea}(\text{O})]^-$  and  $[\text{Mn}^{\text{IV}}\text{H}_3\text{buea}(\text{OH})]$  (Fig. 9).

Similarly, the reaction involving  $[\text{Mn}^{\text{IV}}\text{H}_3\text{buea}(\text{O})]^-$  and  $[\text{Mn}^{\text{II}}\text{H}_3\text{buea}(\text{OH})]^{2-}$  at room temperature afforded a 45(5) : 55(5) mixture of  $[\text{Mn}^{\text{III}}\text{H}_3\text{buea}(\text{O})]^{2-}$  and  $[\text{Mn}^{\text{III}}\text{H}_3\text{buea}(\text{OH})]^-$  (Fig. S7†). All of these reactions gave the products that are expected for one-electron processes, as

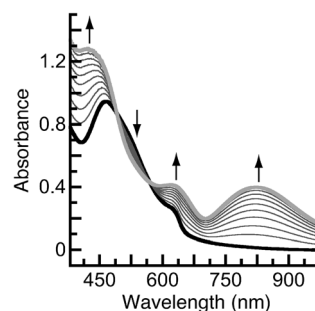


Fig. 7 Electronic absorbance spectra for the reaction in eqn (4):  $[\text{Mn}^{\text{IV}}\text{H}_3\text{buea}(\text{OH})]$  (black) was treated with DBU and  $[\text{FeCp}_2]^+$  at  $-80\text{ }^{\circ}\text{C}$  in THF : DMF to produce  $[\text{Mn}^{\text{V}}\text{H}_3\text{buea}(\text{O})]$  (gray). The peak at  $\sim 620\text{ nm}$  in the starting spectrum is from  $[\text{FeCp}_2]^+$ . Spectra were measured every 30 s.

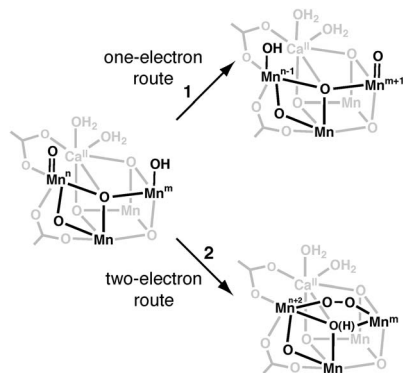


Fig. 8 Possible reaction pathways involving only the Mn–O(H) species within the OEC.

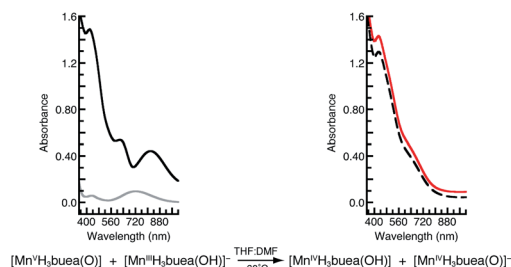


Fig. 9 Electronic absorbance spectra, measured in THF–DMF at  $-60^\circ\text{C}$ , for reactants  $[\text{Mn}^{\text{III}}\text{H}_3\text{buea}(\text{OH})]^-$  (gray) and  $[\text{Mn}^{\text{IV}}\text{H}_3\text{buea}(\text{O})]$  (black, solid), product mixture (red), and a model spectrum showing a 45(5) : 55(5) mixture of  $[\text{Mn}^{\text{IV}}\text{H}_3\text{buea}(\text{O})]^-$  and  $[\text{Mn}^{\text{IV}}\text{H}_3\text{buea}(\text{OH})]$  (black, dashed). The absorbance band from ferrocene (produced in generating the  $\text{Mn}^{\text{V}}\text{-oxo}$  complex) has been subtracted from the spectra.

suggested from our thermodynamic assessments. Furthermore, no reactivity was observed between  $[\text{Mn}^{\text{V}}\text{H}_3\text{buea}(\text{O})]/[\text{Mn}^{\text{IV}}\text{H}_3\text{buea}(\text{OH})]$ ,  $[\text{Mn}^{\text{IV}}\text{H}_3\text{buea}(\text{O})]/[\text{Mn}^{\text{III}}\text{H}_3\text{buea}(\text{OH})]^-$ , and  $[\text{Mn}^{\text{III}}\text{H}_3\text{buea}(\text{O})]^-/[\text{Mn}^{\text{II}}\text{H}_3\text{buea}(\text{OH})]^-$ .

## Discussion

### Preparation and properties of $[\text{Mn}^{\text{IV}}\text{H}_3\text{buea}(\text{OH})]$

Mononuclear  $\text{Mn}^{\text{IV}}\text{-OH}$  complexes are relatively rare,<sup>7</sup> especially those in which related metal–oxo complexes are known. We have found that the  $\text{Mn}^{\text{IV}}\text{-OH}$  complex,  $[\text{Mn}^{\text{IV}}\text{H}_3\text{buea}(\text{OH})]$ , can be prepared *via* three independent routes: (1) direct oxidation of the  $\text{Mn}^{\text{III}}\text{-OH}$  complex,  $[\text{Mn}^{\text{III}}\text{H}_3\text{buea}(\text{OH})]^-$ , (2) protonation of the  $\text{Mn}^{\text{IV}}\text{-oxo}$  complex,  $[\text{Mn}^{\text{IV}}\text{H}_3\text{buea}(\text{O})]^-$ , and (3) a PCET process involving the  $\text{Mn}^{\text{V}}\text{-oxo}$  complex,  $[\text{Mn}^{\text{V}}\text{H}_3\text{buea}(\text{O})]$ . The spectroscopic data, including EPR and XAS spectra, are consistent with the formulation of this complex as a high-spin, mononuclear  $\text{Mn}^{\text{IV}}\text{-OH}$  species. With the preparation of  $[\text{Mn}^{\text{IV}}\text{H}_3\text{buea}(\text{OH})]$ , we now have a unique series of six different Mn–O(H) complexes of the tripodal ligand  $[\text{H}_3\text{buea}]^{3-}$ . These results demonstrate that a single ligand set can support mononuclear Mn complexes spanning four different oxidation states (ii through v) while accommodating oxo and hydroxo

ligands derived from water. The synthetic methods we developed to interconvert between the complexes followed from our thermodynamic predictions and are related to processes that are proposed to occur within the OEC.

### Relevance to the OEC: formation of a $\text{Mn}^{\text{V}}\text{-oxo}$ center

The Mn–O(H) complexes of  $[\text{H}_3\text{buea}]^{3-}$  bear some resemblance to  $\text{Mn}_{\text{A4}}$ , the so-called dangling Mn center in the OEC, in that both systems have highly anionic primary coordination spheres and are surrounded by a network of hydrogen bonds. There has been much debate as to the functional role of the  $\text{Mn}_{\text{A4}}$  center with some suggesting that it is directly involved in the formation of dioxygen from water molecules.<sup>2,3</sup> One plausible mechanism involves a  $\text{Mn}^{\text{V}}$  center with a terminal oxo ligand that is formed from a  $\text{Mn}^{\text{IV}}\text{-OH}$  species in the  $\text{S}_3$  state.<sup>4</sup> Insights gained from our work on synthetic Mn–O(H) complexes provided a possible mechanistic framework for how this conversion can be accomplished. Our thermodynamic analysis agrees with the premise that a  $\text{Mn}^{\text{IV}}\text{-OH}$  species cannot convert to a  $\text{Mn}^{\text{V}}\text{-oxo}$  center *via* a PCET process. The estimate of  $95\text{ kcal mol}^{-1}$  for the  $\text{BDE}_{\text{OH}}$  in  $[\text{Mn}^{\text{IV}}\text{H}_3\text{buea}(\text{OH})]$  illustrates that a  $\text{Mn}^{\text{IV}}\text{-O-H}$  bond is too strong to be homolytically cleaved using species generally found within a protein active site, such as a tyrosyl radical ( $\text{BDE}_{\text{OH}}(\text{Tyr-OH}) = 86\text{ kcal mol}^{-1}$ ).<sup>17,25</sup> A more likely mechanism involves a sequential process in which proton transfer is followed by electron transfer. As we demonstrated for the conversion of  $[\text{Mn}^{\text{IV}}\text{H}_3\text{buea}(\text{OH})]$  to  $[\text{Mn}^{\text{V}}\text{H}_3\text{buea}(\text{O})]$ , initial deprotonation of a  $\text{Mn}^{\text{IV}}\text{-OH}$  center to form a  $\text{Mn}^{\text{IV}}\text{-oxo}$  species would sufficiently lower the one-electron oxidation potential so that oxidation to a transient  $\text{Mn}^{\text{V}}\text{-oxo}$  center could be achieved. We suggest that a similar process could be viable during the  $\text{S}_3 \rightarrow \text{S}_4$  step in the OEC to produce a highly reactive  $\text{Mn}^{\text{V}}\text{-oxo}$  center. In this way, the  $\text{Mn}_{\text{A4}}$  center can form a  $\text{Mn}^{\text{V}}\text{-oxo}$  species *via* controlled proton and electron transfer steps.

### Relevance to the OEC: possible role of a Mn–OH unit in water oxidation

Among the proposed mechanisms for O–O bond formation during water oxidation in the OEC, one of the most popular pathways involves the reaction of a metal-bound nucleophile with an electrophilic Mn–oxo. Establishing the identity of the nucleophile is critical for determining the viability of this mechanism. Towards this end, we considered whether two manganese centers could facilitate the coupling of oxo and hydroxo ligands to form an O–O bond within the context of the thermodynamic relationships established for our series Mn–oxo and Mn–hydroxo complexes. The outcomes of the present work indicated that it is unlikely for a Mn–OH center to be involved in O–O bond formation to afford a peroxo species (Fig. 8, route 2) because of the propensity of Mn–oxo complexes to undergo one-electron processes when treated with Mn–OH complexes (Fig. 4). This prediction was experimentally verified by monitoring reactions involving our synthetic Mn–OH and Mn–oxo complexes. *These types of one-electron processes must be avoided by the OEC* in order to oxidize water to a peroxo intermediate. The  $\text{Mn}_3\text{O}_4\text{Ca}$  cluster within the OEC must facilitate

another route to water oxidation: for instance, a nucleophilic mechanism could still be operative if a Ca–OH unit is involved because it is redox-inactive.<sup>1,3,26</sup> We noted that computational studies have suggested alternative mechanisms for O–O bond formation, including radical coupling routes and ones involving the  $\mu_4$ -oxo ligand that links  $\text{Mn}_{\text{A4}}$  to the  $\text{Mn}_3\text{O}_4\text{Ca}$  cube.<sup>27</sup>

## Conclusions

The catalytic conversion of water to dioxygen is an inherently difficult process that involves the precise movement of 4 electrons and 4 protons. In the OEC, these movements are undoubtedly influenced by the structure of the protein active site. The mechanism for water oxidation is still evolving, with several proposals having been reported.<sup>1–3,26,27</sup> Many proposals suggest that the dangling Mn center is directly involved in the binding of water and its conversion to species that can facilitate O–O bond formation. We have used a series of well characterized Mn–OH and Mn–oxo complexes that approximate some of the structural features of the  $\text{Mn}_{\text{A4}}$  center to investigate the role of this unique Mn center in water oxidation within the OEC. This deconstructive approach<sup>28</sup> allowed us to examine inherent properties of these complexes as they pertain to the OEC. The feasibility of a sequential proton transfer-electron transfer route for converting a  $\text{Mn}^{\text{IV}}\text{–OH}$  complexes to a  $\text{Mn}^{\text{V}}\text{–oxo}$  species, which is a possible transformation in the  $\text{S}_3 \rightarrow \text{S}_4$  step, is described. We provided predictive thermodynamic information and experimental evidence against the involvement of a lower valent Mn–OH species as a nucleophile in water oxidation. The mechanism for water oxidation in the OEC continues to be debated, as does the role of the calcium ion within the  $\text{Mn}_3\text{O}_4\text{Ca}$  cluster. It is possible that a Ca–OH unit could be involved in the initial O–O bond forming steps,<sup>3,26,29a,b</sup> which would be consistent with data found in our study. However, alternative proposals exist,<sup>27</sup> including one that suggests that the  $\text{Ca}^{\text{II}}$  ion serves as a redox modulator within the  $\text{Mn}_3\text{O}_4\text{Ca}$  cluster to facilitate oxidation of the cluster.<sup>30</sup> Delineating the role(s) of the metal centers of the cluster in O–O bond formation requires additional studies.

## Acknowledgements

Acknowledgment is made to the NIH (GM50781 to ASB and GM49970 to MPH) and the Office of Science, Basic Energy Sciences (BES), Division of Chemical Sciences, Geosciences and Biosciences, Department of Energy under Contract no. DE-AC02-05CH11231 (JY) for financial support. Portions of this research were carried out at Stanford Synchrotron Radiation Lightsource (SSRL) BL 7-3. The SSRL Structural Molecular Biology Program is supported by the DOE Office of Biological and Environmental Research, and by the National Institutes of Health, National Center for Research Resources, Biomedical Technology Program (P411RR001209).

## Notes and references

- (a) J. Yano, J. Kern, K. Sauer, M. J. Latimer, Y. Pushkar, J. Biesiadka, B. Loll, W. Saenger, J. Messinger, A. Zouni

- and V. K. Yachandra, *Science*, 2006, **314**, 821; (b) A. Guskov, J. Kern, A. Gabdulkhakov, M. Broser, A. Zouni and W. Saenger, *Nat. Struct. Mol. Biol.*, 2009, **16**, 334; (c) S. H. Kim, W. Gregor, J. M. Peloquin, M. Brynda and R. D. Britt, *J. Am. Chem. Soc.*, 2004, **126**, 7228; (d) J. M. Peloquin, K. A. Campbell, D. W. Randall, M. Evanchik, V. L. Pecoraro, W. H. Armstrong and R. D. Britt, *J. Am. Chem. Soc.*, 2000, **122**, 10926; (e) R. D. Britt, K. A. Campbell, J. M. Peloquin, M. L. Gilchrist, C. P. Aznar, M. M. Dicus, J. Robblee and J. Messinger, *Biochim. Biophys. Acta*, 2004, **1655**, 158; (f) J. P. McEvoy and G. W. Brudvig, *Chem. Rev.*, 2006, **106**, 4455 and references therein; (g) A. Zouni, H. T. Witt, J. Kern, P. Fromme, N. Krauss, W. Saenger and P. Orth, *Nature*, 2001, **409**, 739; (h) J. Kern, J. Biesiadka, B. Loll, W. Saenger and A. Zouni, *Photosynth. Res.*, 2007, **92**, 389; (i) B. Loll, J. Kern, W. Saenger, A. Zouni and J. Biesiadka, *Nature*, 2005, **438**, 1040.
- Y. Umena, K. Kawakami, J.-R. Shen and N. Kamiya, *Nature*, 2011, **473**, 55.
- (a) V. L. Pecoraro, M. J. Baldwin, M. T. Caudle, W. Y. Hsieh and N. A. Law, *Pure Appl. Chem.*, 1998, **70**, 925; (b) A. Grundmeier and H. Dau, *Biochim. Biophys. Acta*, 2012, **1817**, 88; (c) C. S. Mullins and V. L. Pecoraro, *Coord. Chem. Rev.*, 2008, **252**, 416; (d) M. M. Najafpour and Govindjee, *Dalton Trans.*, 2011, **40**, 9076; (e) G. W. Brudvig, *Philos. Trans. R. Soc., B*, 2008, **363**, 1211; (f) J. Messinger, *Phys. Chem. Chem. Phys.*, 2004, **6**, 4764.
- For examples of  $\text{Mn}^{\text{IV}}\text{–OH}$  species suggested in the  $\text{S}_3$  state, see: (a) P. E. M. Siegbahn, *Phys. Chem. Chem. Phys.*, 2012, **14**, 4849; (b) E. M. Sproviero, J. A. Gascón, J. P. McEvoy, G. W. Brudvig and V. S. Batista, *Coord. Chem. Rev.*, 2008, **252**, 395; (c) P. E. M. Siegbahn, *Chem.–Eur. J.*, 2008, **14**, 8290; (d) L. Rapatskiy, N. Cox, A. Savitsky, W. M. Ames, J. Sander, M. M. Nowaczak, M. Rogner, A. Boussac, F. Neese, J. Messinger and W. Lubitz, *J. Am. Chem. Soc.*, 2012, **134**, 16619; (e) T. J. Meyer, M. H. V. Huynh and H. H. Thorp, *Angew. Chem., Int. Ed.*, 2007, **46**, 5284.
- (a) R. Gupta, C. E. MacBeth, V. G. Young Jr. and A. S. Borovik, *J. Am. Chem. Soc.*, 2002, **124**, 1136; (b) C. E. MacBeth, R. Gupta, K. R. Mitchell-Koch, V. G. Jr Young, G. H. Lushington, W. H. Thompson, M. P. Hendrich and A. S. Borovik, *J. Am. Chem. Soc.*, 2004, **126**, 2556; (c) T. H. Parsell, R. K. Behan, M. T. Green, M. P. Hendrich and A. S. Borovik, *J. Am. Chem. Soc.*, 2006, **128**, 8728; (d) T. Taguchi, R. Gupta, B. Lassalle-Kaiser, D. W. Boyce, V. Yachandra, W. B. Tolman, J. Yano, M. P. Hendrich and A. S. Borovik, *J. Am. Chem. Soc.*, 2012, **134**, 1996.
- (a) S. H. Kim, H. Park, M. S. Seo, M. Kubo, T. Ogura, J. Klajn, D. T. Gryko, J. S. Valentine and W. Nam, *J. Am. Chem. Soc.*, 2010, **132**, 14030–14032; (b) Y. Gao, T. Akermark, J. Liu, L. Sun and B. Akermark, *J. Am. Chem. Soc.*, 2009, **131**, 8726.
- (a) G. Yin, A. M. Danby, D. Kitko, J. D. Carter, W. M. Scheper and D. H. Busch, *J. Am. Chem. Soc.*, 2007, **129**, 1512; (b) S. Fukuzumi, H. Kotani, K. A. Prokop and D. P. Goldberg, *J. Am. Chem. Soc.*, 2011, **133**, 1859; (c) T. Kurahashi, A. Kikuchi, T. Tosha, Y. Shiro, T. Kitagawa and H. Fujii,

- Inorg. Chem.*, 2008, **47**, 1674; (d) C. Hureau, E. Anxolabéhère-Mallart, G. Blondin, E. Rivière and M. Nierlich, *Eur. J. Inorg. Chem.*, 2005, 4808; (e) I. Gracia-Bosch, A. Company, C. W. Cady, S. Styring, W. R. Browne, X. Ribas and M. Costas, *Angew. Chem., Int. Ed.*, 2011, **50**, 5648.
- 8 Examples of low-spin  $\text{Mn}^{\text{V}}$ -oxo complexes: (a) Z. Gross, G. Golubkov and L. Simkhovich, *Angew. Chem., Int. Ed.*, 2000, **39**, 4045; (b) K. A. Prokop, S. P. de Visser and D. P. Goldberg, *Angew. Chem., Int. Ed.*, 2010, **49**, 5091; (c) E. N. Jacobsen, W. Zhang, A. R. Muci, J. R. Ecker and L. Deng, *J. Am. Chem. Soc.*, 1991, **113**, 7063; (d) T. J. Collins, R. D. Powell, C. Slebonick and E. S. Uffelman, *J. Am. Chem. Soc.*, 1990, **112**, 899; (e) J. M. Workman, R. D. Powell, A. D. Procyk, T. J. Collin and D. F. Bosian, *Inorg. Chem.*, 1992, **31**, 1548; (f) D. E. Lansky, B. Mandimutsira, B. Ramdhanie, M. Clausen, J. Penner-Hahn, S. A. Zvyagin, J. Telser, J. Krzystek, R. Zhan, Z. Ou, K. M. Kadish, L. Zakharov, A. L. Rheingold and D. P. Goldberg, *Inorg. Chem.*, 2005, **44**, 4485.
- 9 Examples of other  $\text{Mn}^{\text{IV}}$ -oxo complexes: (a) J. T. Groves and M. K. Stern, *J. Am. Chem. Soc.*, 1987, **109**, 3812; (b) J. T. Groves and M. K. Stern, *J. Am. Chem. Soc.*, 1988, **110**, 8628; (c) R. S. Czernuszewicz, Y. O. Su, M. K. Stern, K. A. Macor, D. Kim, J. T. Groves and T. G. Spiro, *J. Am. Chem. Soc.*, 1988, **110**, 4158; (d) J. T. Groves, J. Lee and S. S. Marla, *J. Am. Chem. Soc.*, 1997, **119**, 6269; (e) M. Schappacher and R. Weiss, *Inorg. Chem.*, 1987, **26**, 1190; (f) K. Ayougou, E. Bill, J. M. Charnock, C. D. Garner, D. Mandon, A. X. Trautwein, R. Weiss and H. Winkler, *Angew. Chem., Int. Ed. Engl.*, 1995, **34**, 343; (g) R. D. Arasaingham, G.-X. He and T. C. Bruice, *J. Am. Chem. Soc.*, 1993, **115**, 7985; (h) W. Adam, C. Mock-Knoblauch, C. R. Saha-Möllner and M. Herderich, *J. Am. Chem. Soc.*, 2000, **122**, 9685; (i) D. F. Leto, R. Ingram, V. W. Day and T. A. Jackson, *Chem. Commun.*, 2013, **49**, 5378–5380; (j) X. Wu, M. S. Seo, K. M. Davis, Y.-M. Lee, J. Chen, K.-B. Cho, Y. N. Pushkar and W. Nam, *J. Am. Chem. Soc.*, 2011, **133**, 20088–20091.
- 10 All redox potentials are referenced to the  $[\text{FeCp}_2]^{+/0}$  couple.
- 11 There is also a small, multi-line signal at  $g = 2$  that was from a minority, mixed-valent species that is less than 10% of the total amount of manganese in the sample.
- 12 The signal at  $g = 4.4$  was from slight excess of  $[\text{FeCp}_2]\text{BF}_4$  still present in the reaction mixture. Note that the residual broad signal at  $g = 9.16$  in parallel mode was from an impurity of unknown origin and its amount was preparation dependent.
- 13 The EPR signal for  $[\text{Mn}^{\text{IV}}\text{H}_3\text{buea}(\text{OH})]$  indicates the presence of two  $S = 3/2$  species in a 70/30 ratio, which is unchanged for different solvents and solvent mixtures. Both species display signals that are different from the  $[\text{Mn}^{\text{IV}}\text{H}_3\text{buea}(\text{O})]$  complex. We show that both species can be chemically converted to and from  $[\text{Mn}^{\text{IV}}\text{H}_3\text{buea}(\text{O})]$ – and  $[\text{Mn}^{\text{V}}\text{H}_3\text{buea}(\text{O})]$ . The two  $\text{Mn}^{\text{IV}}$ –OH species are assigned to chemically-equivalent complexes with slightly different conformations of  $[\text{H}_3\text{buea}]^{3-}$  ligand.
- 14 R. Gupta, T. Taguchi, A. S. Borovik and M. P. Hendrich, *Inorg. Chem.*, 2013, **52**, 12568.
- 15 J. M. Mayer, D. L. Thorn and T. H. Tulip, *J. Am. Chem. Soc.*, 1985, **107**, 7454.
- 16  $[\text{Mn}^{\text{IV}}\text{H}_3\text{buea}(\text{OH})]$  has a Jahn–Teller effect that could also influence the bond lengths around the manganese center.
- 17 (a) J. J. Scepaniak, C. S. Vogel, M. M. Khusniyarov, F. W. Heinemann, K. Meyer and J. M. Smith, *Science*, 2011, **331**, 1049; (b) J. M. Smith and D. Subedi, *Dalton Trans.*, 2012, **41**, 1423.
- 18 (a) J. M. Mayer, *Annu. Rev. Phys. Chem.*, 2004, **55**, 363; (b) J. M. Mayer, *Acc. Chem. Res.*, 2011, **44**, 36.
- 19 T. H. Parsell, M.-Y. Yang and A. S. Borovik, *J. Am. Chem. Soc.*, 2009, **131**, 2762.
- 20 A related study using electrochemical methods with a series of monomeric  $\text{Mn}$ –OH<sub>2</sub>,  $\text{Mn}$ –OH, and  $\text{Mn}$ –oxo has been reported: B. Lassalle-Kaiser, C. Hureau, D. A. Pantazis, Y. Pushkar, R. Guillot, V. K. Yachandra, J. Yano, F. Neese and E. Anxolabéhère-Mallart, *Energy Environ. Sci.*, 2010, **3**, 924.
- 21 J. J. Warren, T. A. Tronic and J. M. Mayer, *Chem. Rev.*, 2010, **110**, 6961.
- 22 For example, see: T. A. Betley, Q. Wu, T. Van Voorhis and D. G. Nocera, *Inorg. Chem.*, 2008, **47**, 1849.
- 23 (a) D. W. Christianson, *Acc. Chem. Res.*, 2005, **38**, 191; (b) D. W. Christianson and J. D. Cox, *Annu. Rev. Biochem.*, 1999, **68**, 33.
- 24 (a) C. V. Sastri, J. Lee, K. Oh, Y. J. Lee, J. Lee, T. A. Jackson, K. Ray, H. Hirao, W. Shin, J. A. Halfen, J. Kim, L. Jr Que, S. Shaik and W. Nam, *Proc. Natl. Acad. Sci. U. S. A.*, 2007, **104**, 19181; (b) D. P. Goldberg, *Acc. Chem. Res.*, 2007, **40**, 626; (c) J. M. Mayer, *Acc. Chem. Res.*, 1998, **31**, 441.
- 25 We are aware that the microenvironment within the OEC could influence the tyrosyl O–H bond energy such that they could be different from those observed in our systems.
- 26 V. A. Szalai, D. A. Stone and G. W. Brudvig, in *Photosynthesis: mechanisms and effects*, ed. G. Garab, Kluwer Academic, Dordrecht, The Netherlands, 1998, p. 1403.
- 27 (a) P. E. M. Siegbahn, *Acc. Chem. Res.*, 2009, **42**, 1871; (b) N. Cox, D. A. Pantazis, F. Neese and W. Lubitz, *Acc. Chem. Res.*, 2013, **46**, 1588; (c) N. Cox and J. Messinger, *Biochim. Biophys. Acta*, 2013, **1827**, 1020.
- 28 S. A. Cook and A. S. Borovik, *Nat. Chem.*, 2013, **5**, 259.
- 29 (a) C. F. Yocum, *Coord. Chem. Rev.*, 2008, **252**, 296; (b) T. A. Ono and Y. Inoue, *FEBS Lett.*, 1988, **227**, 147; (c) A. Boussac, J. L. Zimmermann and A. W. Rutherford, *FEBS Lett.*, 1990, **277**, 69.
- 30 J. S. Kanady, E. Y. Tsui, M. W. Day and T. Agapie, *Science*, 2011, **333**, 733.